Available online at www.sciencedirect.com
SCIENCE DIRECT®
Journal of Catalysis 237 (2006) 17–28
JOURNAL OF CATALYSIS
www.elsevier.com/locate/jcat

Preferential CO oxidation in hydrogen (PROX) on ceria-supported catalysts, part II: Oxidation states and surface species on Pd/CeO_2 under reaction conditions, suggested reaction mechanism

O. Pozdnyakova [a], D. Teschner [a,b,*], A. Wootsch [a], J. Kröhnert [b], B. Steinhauer [b], H. Sauer [b], L. Toth [c], F.C. Jentoft [b], A. Knop-Gericke [b], Z. Paál [a], R. Schlögl [b]

[a] *Institute of Isotopes, CRC, HAS, POB 77, Budapest, H-1525, Hungary*
[b] *Department of Inorganic Chemistry, Fritz-Haber-Institut der Max-Plank-Gesellschaft, Faradayweg 4-6, D-14195 Berlin, Germany*
[c] *Research Institute for Technical Physics and Materials Science, HAS, Budapest, POB 49, H-1525, Hungary*

Received 4 September 2005; revised 13 October 2005; accepted 17 October 2005

Available online 17 November 2005

Abstract

The aim of the PROX reaction is to reduce the CO content of hydrogen feed to proton-exchange membrane fuel cells (PEMFCs) by selective oxidation of CO in the presence of excess hydrogen. Both Pt and Pd on ceria are active in CO oxidation (without hydrogen), whereas Pd is poorly active in the presence of hydrogen. In this paper we explore the reasons for such behavior, using the same techniques for Pd/CeO_2 as used for Pt/CeO_2 in Part I: catalytic tests, in situ DRIFTS, high-pressure XPS, HRTEM, and TDS. We also examine the reaction mechanism of CO oxidation (without hydrogen), which does not occur via exactly the same mechanism on Pt and Pd/CeO_2 catalysts. In the presence of hydrogen (PROX) at low temperature ($T = 350$–380 K), the formation of Pd β-hydride was confirmed by high-pressure in situ XPS. Its formation greatly suppressed the possibility of CO oxidation, because oxygen both from gas-phase and support sites reacted rapidly with hydride H to form water, which readily desorbed from Pd. Nevertheless, CO adsorption was not hampered here. These entities transformed mainly to surface formate and formyl (–CHO) species instead of oxidation as observed by DRIFTS. The participation of a low-temperature water–gas shift type reaction proposed for the platinum system (see Part I) was hindered. Increasing temperature led to decomposition of the hydride phase and a parallel increase in the selectivity toward CO oxidation. This still remained lower on Pd/CeO_2 than on Pt/CeO_2, however.

Keywords: Hydrogen purification; Fuel cell; Preferential CO oxidation; PROX; Palladium; Palladium-hydride; Pd/CeO_2; Ceria; High pressure XPS; In situ DRIFT; TDS; HRTEM

1. Introduction

The importance of the PROX reaction has been described in detail in Part I [1]. Briefly, for the proper operation of proton-exchange membrane fuel cells (PEMFCs), as a rule the CO content of the hydrogen feed must be kept under 1–100 ppm [2]. The aim of the preferential oxidation (PROX) reaction is to selectively oxidize CO, reducing its concentration from 1–1.5% to <100 ppm without oxidation of the excess hydrogen present [1,3,4].

Catalyst formulations found to be active in the PROX reaction can be classified as gold-based catalysts [5–8], supported Pt [5,8–12], Rh [9], Ru [9,13], bimetallic Pt–Sn [11,14] and other systems not containing metallic phase, such as CuO/CeO_2 [5,15]. These systems as a rule are also active in low-temperature CO oxidation. Palladium-based catalysts represent a class of its own; whereas Pd on different supports, especially on those active in the transient oxygen storage (such as ceria) is remarkably active in CO oxidation [16–20], it shows very low selectivity toward CO oxidation in the presence of hydrogen [9,21–23].

This low activity/selectivity of Pd in the PROX reaction has not yet been elucidated in detail. One group [9,21] explained

* Corresponding author. Fax: +49 30 8413 4676.
E-mail address: teschner@fhi-berlin.mpg.de (D. Teschner).

0021-9517/$ – see front matter
doi:10.1016/j.jcat.2005.10.015

this by the change in the oxidation state of Pd. The highly active reduced Pd form (active in low-temperature CO oxidation) could be oxidized to PdO_x, which is less active in CO oxidation (without hydrogen). This change occurred around 360 K on Pd/Al_2O_3 in the presence of oxygen [9]. The authors stated that this PdO_x was very active in hydrogen oxidation, whereas it showed low activity in CO oxidation and thus low selectivity in the PROX reaction. They also suggested that other metals, like Au or Pt, cannot be oxidized as easily as Pd, and the rate of CO oxidation on their metallic form was higher than that of H_2 oxidation. This tentative proposition was not supported by any experimental evidence, however.

In the present work we studied the PROX reaction on Pd/CeO_2 catalysts, active in CO oxidation in both the presence [19] and absence of oxygen (OSC) [24,25], using the same experimental methods as in Part I [1]: catalysis, high-pressure XPS, TDS, HRTEM, and in situ DRIFT spectroscopy. The aims of this paper are to clarify the reaction mechanism of both CO oxidation and the PROX reaction on a Pd catalyst, to study the role of the reducible ceria support, and to compare its behavior with that of Pt/CeO_2, which was found to be remarkably active in the PROX reaction [1,12].

2. Experimental

2.1. Catalysts

Two catalysts with nominally 1 and 5% metal loadings were prepared on the same ceria support used in Part I [1] (Rhodia Catalysts & Electronics, France; BET = 96 $m^2\,g^{-1}$ [26]), by wet impregnation with an aqueous solution of $Pd(NH_3)_4(NO_3)_2$ [12,27]. The impregnated samples were dried at 393 K overnight and calcined for 4 h at 773 K in flowing air (30 mL/min), then reduced at 672 K for 4 h in flowing H_2 (30 mL/min). Dispersion was determined by low-temperature (223 K) H_2 adsorption after reduction [28,29]. The received values were $D = 68\%$ for 1% Pd/CeO_2 and 23% for 5% Pd/CeO_2.

2.2. Catalysis

Catalytic tests were carried out in the same atmospheric continuous-flow reactor system as in the studies reported in Part I [1], using stainless steal tubing and connections and analytical-grade gases controlled by mass-flow controllers. Products were analyzed by a gas chromatograph (TCD) equipped with a polar column (Poropak Q) separating CO_2 and H_2O from the other outlet gases, and by a hydrogen-compensated flue-gas analyzer (type MRU DELTA 65-3) for CO and O_2 quantification. Methane formation did not occur on Pd catalysts; CO_2 and H_2O were detected only as products, similar to Pt [1]. The total gas inlet was 100 N mL/min, containing 1% CO, 0.4–1% O_2 (oxygen excess, λ, 0.8–2) and the rest H_2.

The catalysts were activated in situ in flowing air (30 mL/min) at 573 K before catalytic tests. A charge of 95 mg 1% Pd/CeO_2 and 83 mg 5% Pd/CeO_2 was used in the catalytic reactor and reactivated between different measurement series by the aforementioned procedure [12]. CO and O_2 conversion, as well as selectivity, were calculated as described previously [1,12].

2.3. Temperature-programmed desorption

Different gas mixtures were adsorbed at room temperature on the 5% Pd/CeO_2: $CO + O_2$ (10^{-2} mbar $O_2 + 2 \times 10^{-2}$ mbar CO for 20 min) and $H_2 + CO + O_2$ (4.7×10^{-1} mbar $H_2 + 2 \times 10^{-2}$ mbar $CO + 10^{-2}$ mbar O_2 for 20 min). After adsorption, the sample was evacuated and transferred to the UHV part of the setup to follow the desorption pattern (heating rate, 1 K/s). For more details, see Part I.

2.4. In situ diffuse reflectance infrared spectroscopy

DRIFTS experiments were carried out under the same conditions as in Part I [1], with the same Bruker spectrometer. Inlet gases were analytical grade and were controlled by mass-flow controllers. The total gas flow was 50 N mL/min, containing 1% CO in N_2 (referred to as *CO alone*), 1% CO and 1% O_2 in N_2 (*CO + O2*), or 1% CO and 1% O_2 in H_2 (*PROX*).

All measurements were carried out on a ca. 100-mg fresh sample previously pretreated in situ in flowing air (30 mL/min) at 573 K. The catalyst was purged in N_2 while being cooled to the desired reaction temperature of 383 or 523 K. A spectrum of the activated sample before adsorption was collected in N_2 at the reaction temperature, then the reaction mixture—premixed in a bypass—was introduced to the catalyst in a single step. Spectra were collected as a function of time on stream for 90 min in all cases. Only spectra under steady-state conditions are shown here.

The gas composition was analyzed only in the case of the PROX reaction by a mass spectrometer. Selectivity and activity values were calculated using the same formula as presented earlier [1].

2.5. High-pressure X-ray photoelectron spectroscopy

The in situ XPS experiments were performed at beamline U49/2-PGM2 at BESSY in Berlin. Ce 3d, O 1s, Pd 3d, and C 1s spectra were recorded with photon energies of $h\nu = 1035$, 920, 725, and 670 eV. The binding energies (BEs) were calibrated using internal references, such as the Ce 3d V (882.4 eV) and U‴ (916.7 eV) hybridization states or the Ce 4f state in the band gap. Decomposition of the Pd 3d, O 1s, and C 1s regions was performed using Gauss–Lorentz curves, except for the metallic Pd 3d component at 335 eV, which was fitted using a Gauss–Lorentz profile with an exponential tail. The 5% Pd/CeO_2 pellet ($\sim$100 mg) was activated in situ in oxygen (0.5 mbar, 573 K). The PROX mixture contained 0.45 mbar H_2, 0.031 mbar CO, and 0.015 mbar O_2. Gas-phase analysis was carried out using a quadrupole Balzers mass spectrometer. For more details, see Part I.

2.6. High-resolution transmission electron microscopy

HRTEM investigations were performed with a Philips CM200 FEG electron microscope operated at 200 keV. The microscope

was equipped with a Gatan GIF 100 imaging filter, a Gatan Slow-Scan camera, and an EDX system. The sample was prepared from a piece of 5% Pd/CeO_2 that was previously activated in O_2 and used in the PROX mixture in the in situ XPS cell (as was done for the in situ XPS experiments).

3. Results

3.1. Catalytic reaction

Fig. 1 shows the CO oxidation activity on the 1% Pd/CeO_2 catalyst in the absence of hydrogen. The sharp "light off" observed on Pt/CeO_2 [1] was also found here when excess oxygen was used (Fig. 1), whereas it was less pronounced on Pd when $\lambda \leqslant 1$ was applied than on Pt under the same conditions.

In the presence of hydrogen (Fig. 2), the oxygen conversion was very high on Pd/CeO_2—around 98–100%—similar to that on Pt/CeO_2 [1,12]. In contrast, the CO conversion was very low on Pd/CeO_2 and increased as a function of temperature, as opposed to Pt/CeO_2 [1,12]. This increase was rather steep up to 380 K, after which only little variation was observed. Interestingly, the CO conversion was almost independent of the oxygen excess used (Fig. 2a). Fig. 2d presents hydrogen conversion values calculated as the consumption of the inlet excess hydrogen. Their nominally low values are due to the high hydrogen excess present in the inlet stream. Hydrogen oxidation was enhanced by the higher excess of oxygen, that is, by higher $p(O_2)$. Because the CO conversion was more or less independent of λ, the CO_2 selectivity pattern (Fig. 2c) was dictated by the enhanced hydrogen conversion at higher oxygen excess. The actual selectivity values (Fig. 2c) were much lower on Pd than on Pt, in good agreement with earlier data [9,21–23].

Similar to the methodology used in Part I, the 5% Pd/CeO_2 catalyst was measured in the high-pressure XPS apparatus, the 1% catalyst was evaluated in DRIFTS experiments, and both catalysts were tested in the catalytic reactor. The results, which

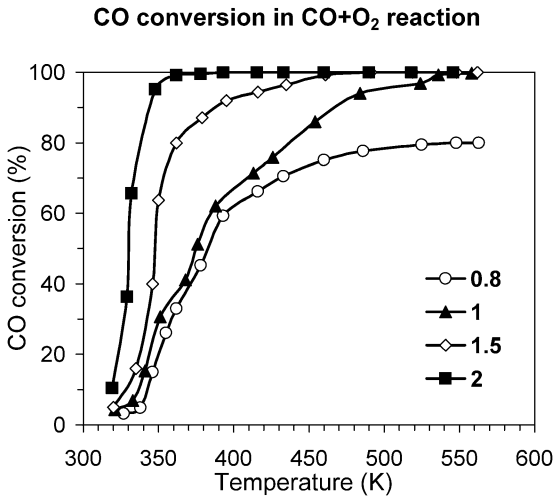

Fig. 1. Conversion of carbon monoxide on 1% Pd/CeO_2 at different oxygen excess, λ (in the absence of hydrogen).

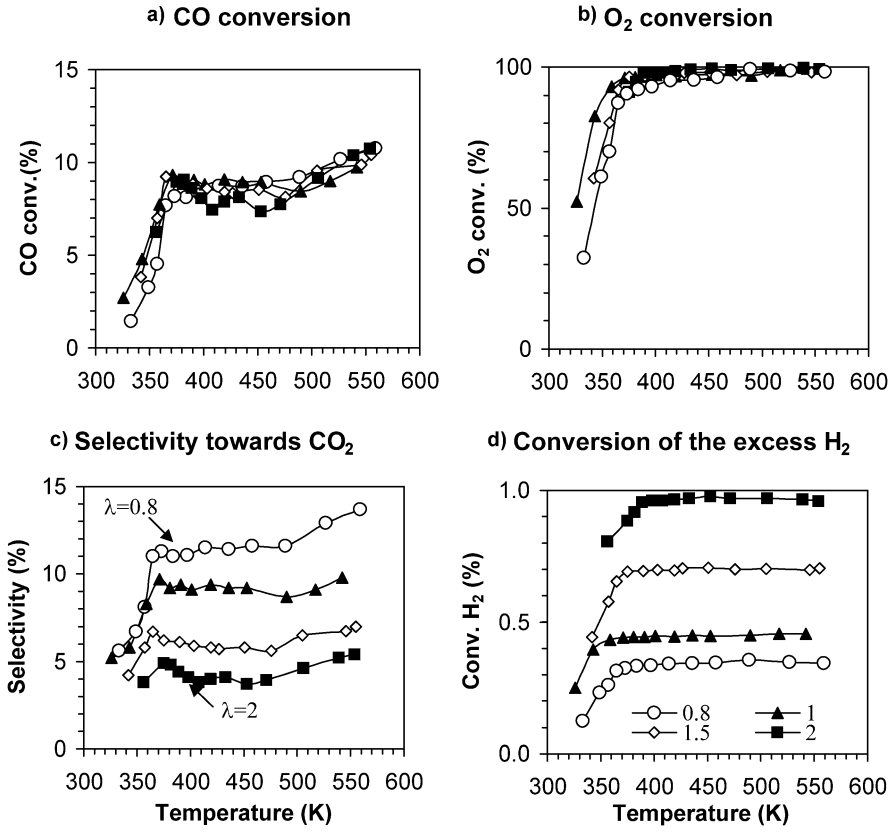

Fig. 2. The PROX reaction on 1% Pd/CeO_2 catalyst at different oxygen excess, λ. CO oxidation activity in the presence of hydrogen (a), oxygen conversion (b), selectivity towards CO oxidation (c), and conversion of the excess hydrogen (d).

Table 1
PROX reaction in different experimental setups and on different catalysts. Reaction mixtures contained 1% CO, 0.5 or 1% O_2 (O_2 excess $\lambda = 1$ or 2) in H_2. Total pressure: $p = 1$ atm in catalytic reactor and DRIFT cell and $p = 0.5$ mbar in high pressure XPS

	Catalytic reactor								DRIFTS		XPS	
	1% Pd/CeO_2				5% Pd/CeO_2				1% Pd/CeO_2		5% Pd/CeO_2	
O_2 excess (λ)	1	1	2	2	1	1	2	2	2	2	1	1
T (K)	383	523	383	523	383	523	383	523	383	523	358	523
X_{CO} (%)	9	9	9	10	10	11	9	12	4	10	1	8
S (%)	9	9	5	5	10	11	5	6	3	6	6	17
X_{O2} (%)	96	99	98	100	97	100	99	100	70	82	14	53

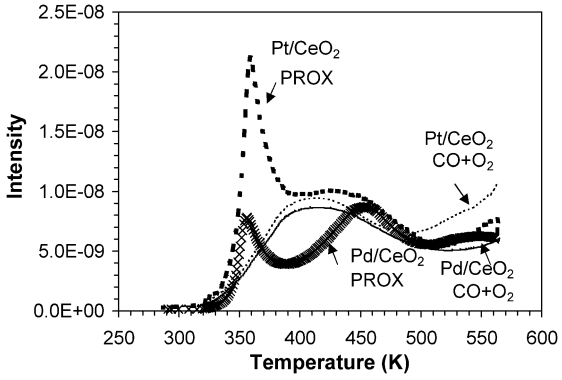

Fig. 3. Temperature programmed desorption (TDS) curves of CO_2 from the 5% loading catalysts after adsorbing different gas mixtures at room temperature: $CO + O_2$ 10^{-2} mbar $O_2 + 2 \times 10^{-2}$ mbar CO for 20 min, and PROX mixture 4.7×10^{-1} mbar $H_2 + 2 \times 10^{-2}$ mbar $CO + 10^{-2}$ mbar O_2 for 20 min. Pt/CeO_2 in $CO + O_2$, thin dashed line. Pt/CeO_2 in PROX, thick dashed line. Pd/CeO_2 in $CO + O_2$, thin full line. Pd/CeO_2 in PROX, ×××.

are compared in Table 1, show that the activity pattern exhibited similar trends, albeit different actual values. In the catalytic reactor, the almost total oxygen conversion was accompanied by ca. 10% CO conversion independent of the reaction conditions. In the spectroscopic apparatus, the lower contact time (and much higher dead volumes than in the catalytic reactor [1]) manifested itself in lower oxygen conversion values.

Summarizing the catalytic results, Pd/CeO_2 catalysts showed much lower selectivity toward CO oxidation in the presence of hydrogen than Pt/CeO_2, especially at low temperatures (365–385 K), at about the same high oxygen conversion, using approximately the same mass of catalyst with about the same dispersion. In contrast, this formulation was active in CO oxidation without hydrogen (Fig. 1).

3.2. Temperature-programmed desorption

Fig. 3 shows the desorption curves of CO_2 for 5% Pd/CeO_2 after adsorbing different gas mixtures at ambient temperature. For comparison, the figure also includes the corresponding data for the platinum catalyst. Both catalysts reveal very similar CO_2 desorption curves when no hydrogen was added, with a broad first maximum at ∼400 K and a second maximum at or above 573 K. The first maximum is attributed to formation of CO_2 on metallic particles; the second is due to CO_2 desorbing from the support. In the presence of hydrogen, however, (i) the first broad peak separates into two peaks, a narrow one at lower (∼360 K) and a second one at higher temperature (∼440–450 K); (ii) the amount of CO_2 desorbing in the narrow peak is roughly three times less for Pd/CeO_2 than for Pt/CeO_2; and (iii) the desorption pattern above 450 K is the same for the two samples. Water formation was similar for both catalysts (slightly lower for Pd), whereas a significant amount of hydrogen desorbed from Pd/CeO_2 (data not shown).

3.3. In situ DRIFTS

3.3.1. DRIFT spectra in the 2200–1800 cm^{-1} region

Fig. 4 shows the DRIFT spectra of 1% Pd/CeO_2 at 383 K and 523 K under CO alone, $CO + O_2$, and PROX conditions in the 2200–1800 cm^{-1} region. Bands observed were denoted following the original assignments of Palazov et al. [30]. Adsorption of CO alone (Fig. 4a) produced strong bands at 2082 cm^{-1} (L_2) (with significant broadening at the low-frequency side) and ca. 1971 cm^{-1} (B_2), as well as weak bands at 2177, 2152, and 2135 cm^{-1} (L_3). The broad tail toward lower wavenumbers of the strong L_2 band contained a component at ca. 2065 cm (L_1). The ν(CO) bands above 2000 cm^{-1} were attributed to terminal, mono-coordinated, or linearly bonded carbon monoxide, whereas the broad, convoluted bands under 2000 cm^{-1} were assigned to multicoordinated CO [31]. The L_2 and L_3 bands were ascribed to the linear adsorption of CO on Pd^0 and Pd^{n+} sites, respectively [26]. The asymmetrical broad B_2 band was attributed to the bridged adsorption of CO on Pd^0 sites. The doublet encompassing weak broad bands at 2177 and 2152 cm^{-1} was ascribed to CO linearly adsorbed on oxidized ceria sites [32], overlapping with the gas-phase CO.

Increasing temperature led to (i) almost complete disappearance of the L_2 and L_1 bands, (ii) appearance of a broad feature at 2115 cm^{-1}, and (iii) a shift of the B_2 band toward lower wave-numbers (from ca. 1971 to ca. 1945 cm^{-1}). The broad feature at ∼2115 cm^{-1} may encompass contributions from CO stretching on Ce^{3+} as well as on Pd^{n+} sites.

The presence of oxygen in the gas mixture (Fig. 4b) did not affect the position and intensities of the ν(CO) bands at $T = 383$ K, whereas at elevated temperatures, no bands of multicoordinated CO were seen, and a general decrease in the band intensities was observed.

Under PROX conditions at $T = 383$ K, the broad L_1 band with an additional feature at ca. 2044 cm^{-1} dominated the spectra, whereas L_2 was obscured by the intensive L_1 band, and the intensity of B_2 decreased significantly, with a very broad

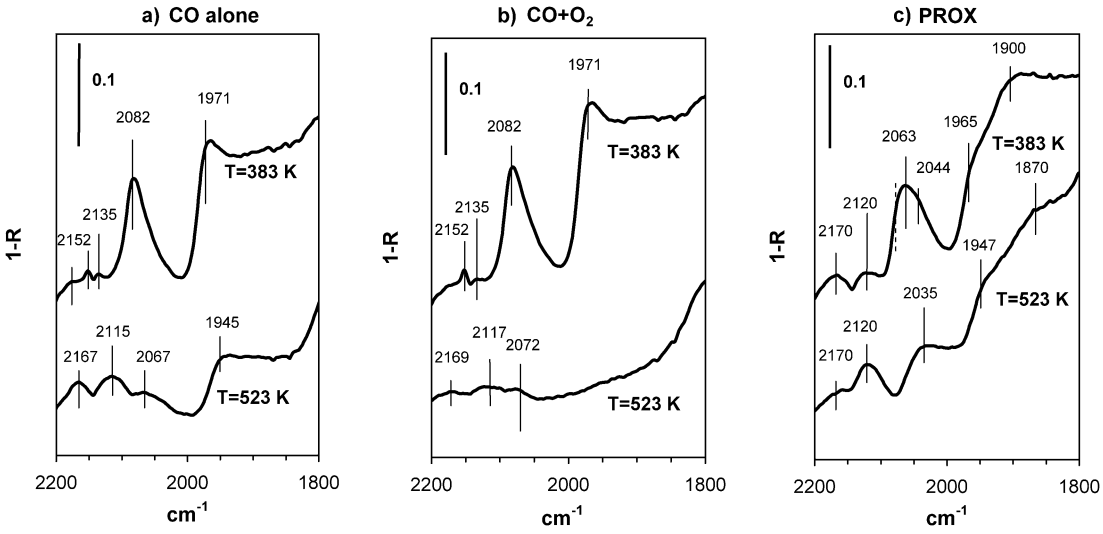

Fig. 4. DRIFT spectra in the 2200–1800 cm^{-1} region (CO vibrations) of 1% Pd/CeO_2 in the presence of (a) 1% CO alone in N_2, (b) in 1% CO and 1% O_2 in N_2, and (c) in 1% CO and 1% O_2 in H_2 (PROX) at 383 and 523 K, respectively.

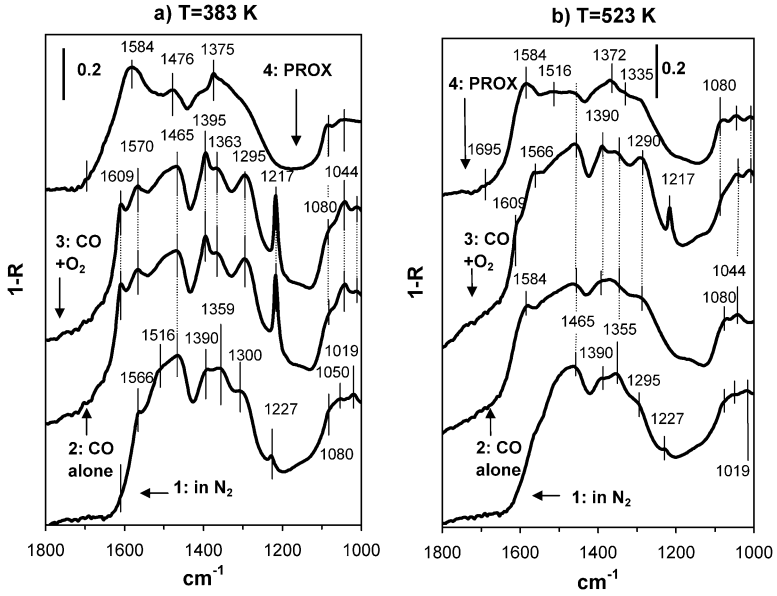

Fig. 5. DRIFT spectra in the 1800–1000 cm^{-1} region (OCO vibrations) of 1% Pd/CeO_2 at (a) $T = 383$ K and (b) $T = 523$ K after activation, in the presence of 1% CO alone in N_2, in 1% CO and 1% O_2 in N_2, and in 1% CO and 1% O_2 in H_2 (PROX), respectively.

band formed at ca. 1900 cm^{-1} (B_1). Increasing temperature in the presence of hydrogen led to (i) a general decrease in intensities and a shift of the bands to lower wavenumbers (main band, from 2063 to ca. 2035 cm^{-1}; B_1 band, from 1900 to ∼1870 cm^{-1}; B_2 band, from 1965 to 1947 cm^{-1}), and (ii) a decrease in the relative intensity of the broad feature observed at ca. 2170 cm^{-1} (ν(CO) on Ce^{4+} sites) and an increase of that at ca. 2120 cm^{-1}. The range of positions observed for the B and L bands may be due to changes in the CO coverage on different experimental conditions [31,33,34]. Downshift and decreased intensity of B bands at higher temperatures and in the presence of H_2 as well as decreased relative intensity of the L_2 band, and increased intensity of the L_1 band in the presence of H_2 at $T = 383$ K indicate lower CO coverage at higher temperatures and in H_2-rich atmosphere.

3.3.2. *DRIFT spectra in the 1800–1000 cm^{-1} region*

Similar to the Pt/CeO_2 catalyst [1], a large variety of carbonate species (OCO vibrations) are present on the O_2 pretreated sample (Fig. 5). Mainly unidentate and/or polydentate carbonate (giving strong bands at 1465 and 1359 cm^{-1} and a weak band at 1080 cm^{-1}) and traces of bidentate carbonate (bands at 1566, 1300, and 1019 cm^{-1}), bicarbonate (medium bands at 1390 and 1227 cm^{-1} and weak bands at ca. 1609 and 1050 cm^{-1}) and carboxylate (1516 cm^{-1}) species are present on the surface of the O_2 pretreated sample at $T = 383$ K. Increasing temperature (Fig. 5b) resulted in a decrease of the bicarbonate and bidentate carbonate species on the surface of the activated sample.

Exposure to CO alone or in the presence of oxygen at $T = 383$ K (Fig. 5a) yields bands characteristic of bicarbon-

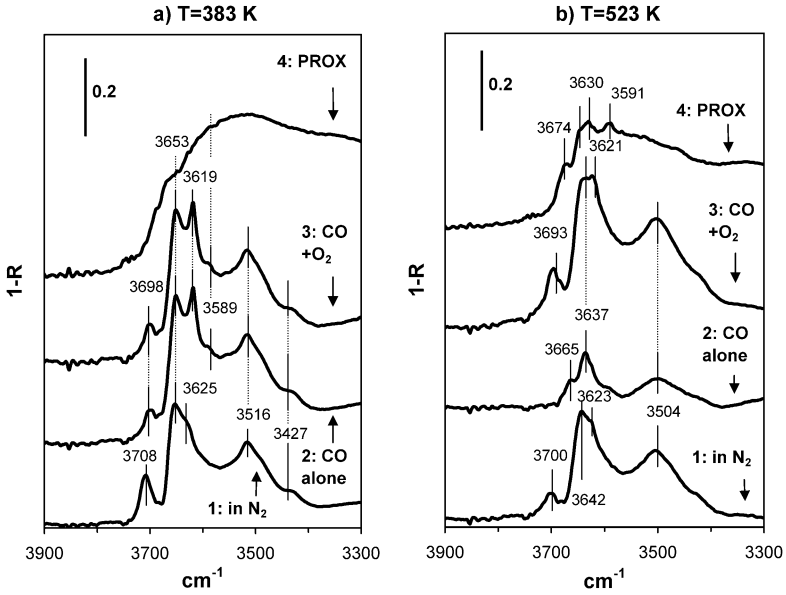

Fig. 6. DRIFT spectra in the 3900–3300 cm^{-1} region (OH vibrations) of 1% Pd/CeO_2 at (a) $T = 383$ K and (b) $T = 523$ K after activation, in the presence of 1% CO alone in N_2, in 1% CO and 1% O_2 in N_2, and in 1% CO and 1% O_2 in H_2 (PROX), respectively.

ate species (strong bands at 1609, 1395, and 1217 cm^{-1} and a medium band at 1044 cm^{-1}) and bidentate carbonate species [$\nu(CO_3)$ bands at 1570 and 1295 cm^{-1}]. Under PROX conditions, bicarbonate species, which were observed in the H_2-free gas mixture, do not form, whereas $\nu(CO_3)$ bands of unidentate and bidentate carbonate species of the same intensities are present in the spectra. At the same time, the spectrum became dominated by a strong broad band centered at ca. 1584 cm^{-1} and medium band at 1375 cm^{-1}. These bands were assigned to ν_{as}(OCO) and δ(CH) vibrations of bridged formate species on the ceria surface. Accordingly, a strong ν(CH) band at 2838 cm^{-1} appeared (Fig. 7). The ν_s(OCO) band of bridged formate species was poorly resolved at ca. 1330 cm^{-1}.

At $T = 523$ K, the presence of CO alone over Pd/CeO_2 did not significantly affect the positions and intensities of the bands corresponding to different carbonate species present on the surface (Fig. 5b). An additional feature at ca. 1584 cm^{-1} appeared, which is assigned to ν_{as}(OCO) vibration of bridged formate species, further supported by the appearance of a strong ν(CH) band at 2847 cm^{-1} (Fig. 7). Exposure to the CO + O_2 gas mixture at $T = 523$ K resulted in spectra very similar to that observed at $T = 383$ K, except that the bands of bicarbonate species were of significantly lower intensities. Under PROX conditions at elevated temperature, a slight decrease in the intensities of the ν_{as}(OCO) and δ(CH) bands of formate species at 1584 and 1372 cm^{-1}, respectively, was observed compared with those in PROX conditions at $T = 383$ K. The small feature at 1335 cm^{-1} with the weak band at 1516 cm^{-1} and the small contribution (1695 cm^{-1}) on the broad shoulder at ca. 1600 cm^{-1} reflect the presence of carboxylate and protonated carboxylate species on the surface.

3.3.3. *DRIFT spectra in the 3900–3300 cm^{-1} region*

After oxidative pretreatment of the 1% Pd/CeO_2 sample, mainly three OH groups at 3708 cm^{-1} (with a weak band at 3684 cm^{-1}), 3653 cm^{-1} (with a shoulder at 3625 cm^{-1}), and 3516 cm^{-1} (with a shoulder at 3427 cm^{-1}) were resolved as shown in Fig. 6. The sharp band at 3708 cm^{-1} was assigned to mono-coordinated OH (I) groups, the broad band at 3653 cm^{-1} and the shoulder at ca. 3625 cm^{-1} were assigned to two types of doubly bridging OH groups (II-A and II-B, respectively), and a broad band centered at 3516 cm^{-1} was assigned to triply bridging OH (III) species [35]. Increase of the temperature resulted in a slight (~10 cm^{-1}) downshift of all ν(OH) bands and a decrease in the number of mono-coordinated (OH-I) hydroxyl groups on the ceria surface.

Exposure to CO at $T = 383$ K over Pd/CeO_2 resulted in the immediate appearance of a strong ν(OH) band at 3619 cm^{-1} and a weak broad band at ca. 3589 cm^{-1}, along with a significant decrease in intensity and a shift to lower (3698 cm^{-1}) wavenumbers of the ν(OH-I) band. The development of a strong band at 3619 cm^{-1} and the decay of the band at 3708 cm^{-1} were attributed to the formation of HCO_3^- species [accordingly to the corresponding $\nu(CO_3)$ bands in Fig. 5] through reaction of CO with terminal (OH-I) hydroxyl groups. The presence of oxygen had no effect on the positions and relative intensities of the ν(OH) bands of isolated OH groups. On CO adsorption at elevated temperature, ν(OH) bands were downshifted as compared with those $T = 383$ K, with a significant decrease in the intensities of the ν(OH-I) and ν(OH-II) bands (Fig. 6b). In the presence of oxygen, more intense bands were observed.

On introduction of the PROX gas mixture at $T = 383$ K, isolated peaks convoluted into intense and broad absorption features that were difficult to follow individually, similar to Pt/CeO_2 [1]. We attributed this feature to adsorbed water (with hydrogen bonding to surface OH groups and to each other) on the ceria surface in the case of Pt/CeO_2. Its overall intensity was lower on Pd/CeO_2 than on Pt/CeO_2. At $T = 523$ K, however, three well-resolved bands of isolated OH groups were observed

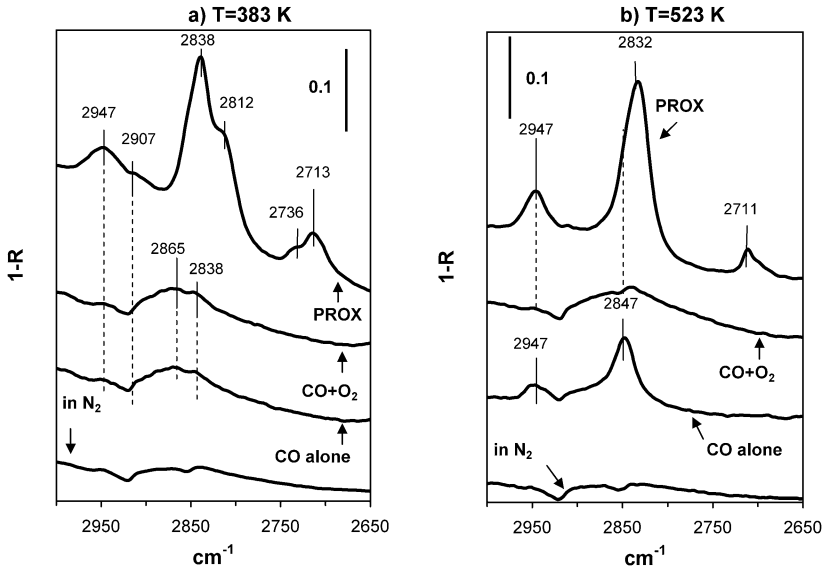

Fig. 7. DRIFT spectra in the 3000–2650 cm^{-1} region (CH vibrations) of 1% Pd/CeO_2 at (a) $T = 383$ K and (b) $T = 523$ K after activation, in the presence of 1% CO alone in N_2, in 1% CO and 1% O_2 in N_2, and in 1% CO and 1% O_2 in H_2 (PROX), respectively.

at 3674 (denoted as OH-IIA*), 3630 (OH-IIB), and 3591 cm^{-1}. Shoulders and less well-defined absorption features were also observed, among which those centered at ca. 3648 (OH-IIB*), 3520, 3450, and 3320 cm^{-1} were the most visible. The difference between the ν(OH) (II-B) and (II-B*) wavenumbers (3630 and 3648 cm^{-1}) may be due to different cerium oxidation states [35] involving surface or subsurface reorganization [35,36]. The ν(OH) band at 3591 cm^{-1} indicates the presence of protonated carboxylate species (–COOH) on the surface of ceria support.

3.3.4. *DRIFT spectra in the 3000–2650 cm^{-1} region*

After oxidative treatment of the Pd/CeO_2 sample, no bands were observed in the 3000–2600 cm^{-1} region, whereas exposure to CO alone or in the presence of oxygen at $T = 383$ K gave weak broad absorption features at ca. 2880–2840 cm^{-1} (Fig. 7). Under steady-state PROX conditions, a strong band at 2838 cm^{-1} (with a well-resolved shoulder at 2812 cm^{-1}) and weaker broad bands at 2947, 2907, 2736, and 2713 cm^{-1} were observed. The main bands were assigned to formate species on the ceria surface [37–39] as follows: 2838 cm^{-1} as ν(CH), 2947 cm^{-1} as a combination of ν_{as}(OCO) at ∼1580 cm^{-1} (Fig. 5) and the C–H in-plane vibration, and 2736 cm^{-1} as an overtone 2δ(C–H) [δ(C–H) ∼1375 cm^{-1} in Fig. 5]. The pronounced shoulder at 2812 cm^{-1} and the broad band centered at 2713 cm^{-1} could be due to C–H stretching vibrations of formyl species [38].

Increasing temperature under conditions of CO alone resulted in a ν(CH) band at 2847 cm^{-1} and a combination mode band at 2947 cm^{-1} (Fig. 7b). In the presence of oxygen at elevated temperature, no distinct bands were resolved in this region. Under PROX conditions at $T = 523$ K, the position of the maximum of the ν(CH) band shifted to 2832 cm^{-1} (with a poorly resolved shoulder at ca. 2848 cm^{-1}), the band of the formyl species at 2812 cm^{-1} was no longer resolved, and that at 2713 cm^{-1} decreased and shifted to 2711 cm^{-1}.

3.4. *High-pressure XPS*

The same procedure was carried out with the palladium sample as described for Pt/CeO_2 [1]: activation in 0.5 mbar O_2 at 573 K, cooling in O_2, and exchange of oxygen to hydrogen (0.45 mbar) at ∼340 K. At room temperature, first CO (0.031 mbar) and then O_2 (0.015 mbar) were added to the hydrogen. The reaction was run with this mixture at 358 and 523 K. The surface state of the sample was investigated in these different environments. The catalytic activity observed during high-pressure XPS measurements is presented in Table 1.

Fig. 8 depicts part of the Ce 3d region in oxygen (at 573 K), in hydrogen (at 300 K), and in the PROX mixture. The cerium 3d signal of Pd/ceria behaved in these different conditions very similar as it did in the case of Pt/ceria, indicating that the surface state of ceria is not affected by the different nature of precious metal particles. Ce was in the +4 state in oxygen; hydrogen induced the reduction of the topmost layer to Ce^{3+}. In the PROX mixture, Ce was almost completely reoxidized. The only difference was that at 358 K in the PROX mixture, cerium in Pd/CeO_x was slightly more oxidized, and no further oxidation occurred at 523 K.

Activation of the sample in O_2 at 573 K brought the palladium particles in an almost completely oxidized PdO_2 state seen by the 2.6-eV BE shift (with respect to the metallic state) in Fig. 9. Tailing in the low-BE side may be caused by some partly reduced states; however, an asymmetric broadening of the PdO_2 peak by differential charging cannot be excluded. Charging of ∼8 eV was observed in O_2, whereas it was as low as 2 eV in the PROX mixture. Hydrogen introduced at 340 K reduced a part of the palladium. Metallic-like Pd (∼335.3 eV) was predominant over PdO_2 during reaction at 358 K. At higher reaction temperatures, the contribution of PdO_2 decreased, whereas the low-BE component shifted −0.25 eV to 335.05 eV, that is, to the position of bulk metallic palladium. Closer inspection of the low-BE component revealed that its shape was roughly symmetric at

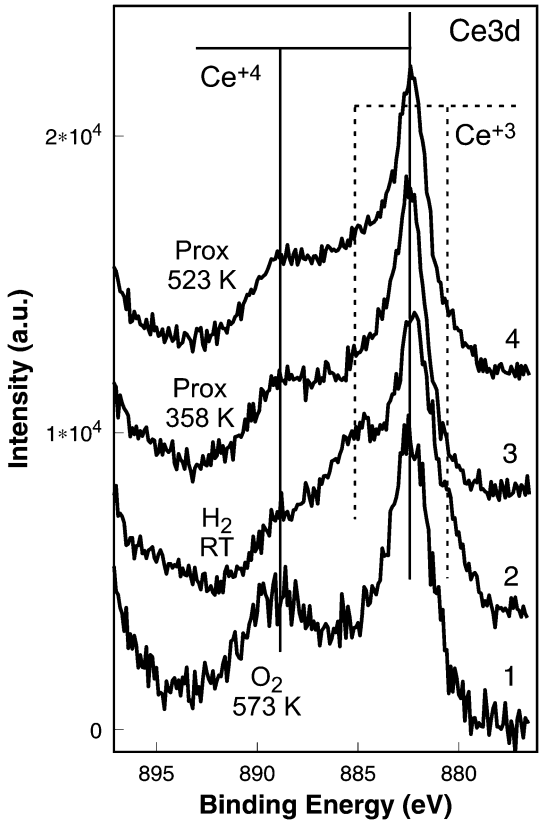

Fig. 8. Part of the Ce 3d region of the 5% Pd/CeO_2 at different conditions: **1**, in 0.5 mbar O_2 at 573 K; **2**, in 0.48 mbar H_2 at RT; **3**, in ∼0.5 mbar PROX mixture at 358 K; **4**, in ∼0.5 mbar PROX mixture at 523 K; the measurements were carried out in sequence as indicated by the numbers.

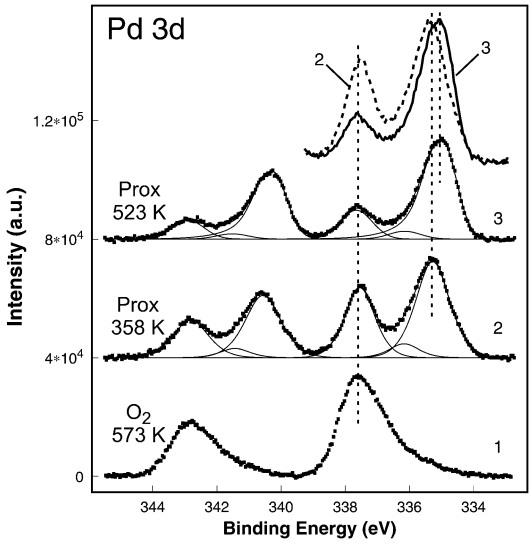

Fig. 9. Pd 3d region of 5% Pd/CeO_2 at different conditions: **1**, in 0.5 mbar O_2 at 573 K; **2**, in ∼0.5 mbar PROX mixture at 358 K; **3**, in ∼0.5 mbar PROX mixture at 523 K.

358 K, and the well-known asymmetry of Pd 3d evolved only at higher temperatures (see the upper part of Fig. 9). The different form and BE position of the low-BE component can be well explained by the formation of a hydride-like structure in the excess of hydrogen at low temperatures, which decomposes at elevated temperature [40]. Formation of β-hydride is effectively enhanced by the limited size of nanoparticles [41], by the presence of adsorbed CO that promotes H bulk dissolution as it reduces the H diffusion barrier between surface and subsurface sites by about 50% [42], and by the hindrance of oxygen diffusion from the PdO_2 core remaining below the metallic shell of Pd particles. Nondestructive depth profiling on the Pd 3d core level (by using different excitation energies and thus different photoelectron kinetic energies) indicated that PdO_2 was at least partly below the low-BE component, that is, below the hydride. As surface hydride decomposed, the further reduction of PdO_2 was more effective. Curve fitting of the PROX spectra provided an intermediate BE component at ∼336.1 eV. Considering the surface core level shift of 0.94–0.99 eV when CO was linearly adsorbed on palladium single crystals [43–45], the small 336.1-eV peak can be attributed to surface palladium atoms adsorbing CO. Thus, the Pd 3d spectra did not indicate the presence of a high amount of adsorbed CO on palladium.

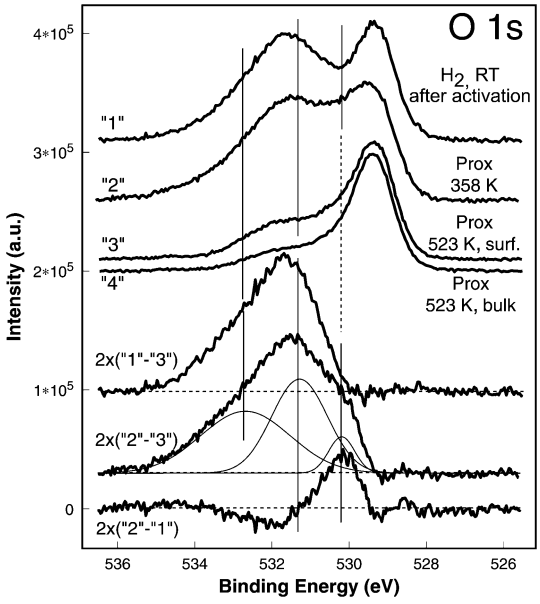

Fig. 10. O 1s spectra of 5% Pt/CeO_2 at different conditions: **1**, in 0.48 mbar H_2 at RT (after O_2 activation at 573 K); **2**, in ∼0.5 mbar PROX mixture at 358 K; **3**–**4**, in ∼0.5 mbar PROX mixture at 523 K; **3**: measured with surface sensitive (650 eV) photon energy (as **1** and **2**, as well) while **4** was measured with more bulk sensitive energy (920 eV). Some difference spectra are also shown.

The carbon 1s spectrum of Pd/ceria in the PROX mixture at 358 K (not shown) revealed a similar picture as the platinum sample at 523 K, with a high amount of graphite/C–H and a low amount of adsorbed CO. The only difference was that the component at about 288.2 eV (most probably surface formates) was more pronounced for Pd/CeO_x.

In Part I we concluded that surface water species are formed during the reaction, which can play a crucial role in the oxidation mechanism. Therefore, we discuss the O 1s spectra of both catalysts in this part. The upper part of Fig. 10 depicts selected O 1s spectra of Pt/ceria at different conditions, whereas the lower part shows some difference spectra. Spectra 1–3 were taken with surface sensitive photon energies, whereas spectrum 4, the same reaction condition as 3, was measured with a more bulk-sensitive photon energy. Comparing spectra 3 and

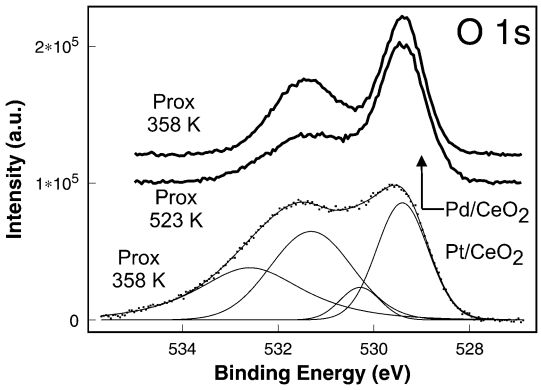

Fig. 11. Comparison of O 1s spectra of 5% Pt/CeO_2 and 5% Pd/CeO_2 in PROX mixture.

4 confirms that the high-BE part of the O 1s spectrum belongs to surface species. Therefore, the peak at 529.4 eV corresponds to oxygen in the ceria lattice (bulk oxygen), in agreement with earlier studies [46,47]. The O-to-Pt atomic ratio was roughly in the range of 100; thus all of the information in the high-BE side of O 1s should necessarily correspond to the surface of ceria. (Changes in the oxygen spectra on a scale of 0.2–1% are not distinguishable.) In hydrogen a strongly pronounced broad peak overlapped with the lattice oxygen component, indicating the presence of OH groups on the surface. This peak was asymmetrically broadened to the high-BE side, as seen in the upper difference curve, involving already surface water. (As shown by the DRIFTS data, different carbonates exist on the surface of ceria already in the activated state, which should contribute to this part of the O 1s signal.) Introduction of $CO + O_2$ to the hydrogen (and heating to 358 K) resulted in a small loss of intensity in the OH region, and a new component at ∼530.2 eV appeared. This feature corresponds to some newly formed oxygenate from CO on the support. Interestingly, the reoxidation of ceria (see Ce 3d) was not accompanied by a significant loss of OH groups; therefore, the presence of OH groups does not necessarily indicate that cerium is in the +3 oxidation state. Heating to 523 K gradually removed most of the high-BE components. Fig. 11 shows the O 1s spectra of Pd/ceria during the reaction, together with the low T spectrum of the platinum sample. The relative intensity of the surface components was considerably lower on Pd/ceria, and in particular, the components at 530.2 and 532.7 eV were missing. The latter peak corresponded to water. Its lower amount points to the importance of surface water in the reaction mechanism, because Pd/ceria is ineffective in removing CO in conditions of hydrogen excess. The difference between the O 1s spectra of the two samples was much smaller at higher temperatures (compare Figs. 10 and 11).

3.5. *High-resolution TEM*

High-resolution TEM measurements were carried out on the postreaction 5% Pd/CeO_x sample (used in the XPS cell at 0.5 mbar PROX mixture at 358 K). Some of the ceria particles remained in the oxidized CeO_2 state (mainly with some lattice distortion), but some were reduced. However, crystalline Ce_2O_3 was not observed. Fig. 12 depicts a typical reduced ceria particle with its power spectrum. After fast Fourier transformation of the selected part of the image, the power spectrum indicated inverse lattice fringes not permitted in CeO_2. Comparison with possible partially reduced ceria phases revealed the presence of $CeO_{1.695}$, in which the ordering of oxygen vacancies led to the formation of a supercell structure with a lattice constant slightly more than twice that of CeO_2 [48]. Some of the reflections were indexed in the power spectrum for the $CeO_{1.695}$ phase. The fraction of reduced ceria was less in Pd/CeO_x compared with the platinum sample after the same reaction treatment.

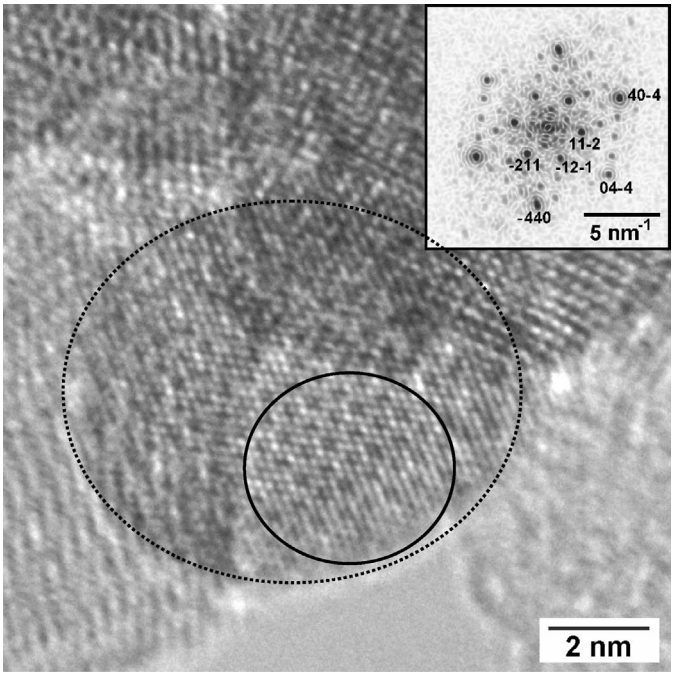

Fig. 12. High-resolution TEM image of 5% Pd/CeO_2 after PROX reaction at 358 K. The inset shows the power spectrum of the selected area (full circle) revealing a partly reduced ceria particle ($CeO_{1.695}$). The dotted line indicates the dimension of the reduced ceria particle.

4. Discussion

Ceria-supported Pt and Pd catalysts are both active in low-temperature CO oxidation [16–20]; compare the results on Pt/CeO_2 in Part I [1] and on Pd/CeO_2 in Fig. 1. However, Pd/CeO_2 exhibited a much lower activity in CO oxidation reaction when carried out in the presence of excess hydrogen (PROX) [9,21–23]; compare the catalytic results presented on Pt/CeO_2 in Part I [1] and on Pd/CeO_2 in Fig. 2. In this paper we aimed to explain these large differences, considering surface species, oxidation states, and reaction mechanism.

The first principal question is whether CO oxidation (without hydrogen) occurs via the same mechanism on Pt and Pd/ceria catalysts. It was concluded [1] that the CO coverage is rather high on Pt particles and that oxygen from support sites promotes CO_2 formation in both CO alone and $CO + O_2$. In the latter case, gas-phase oxygen can reoxidize the ceria surface.

In the case of preoxidized Pd/CeO_2, fewer CO molecules are adsorbed on the metal particles, estimated from the DRIFTS results (Fig. 4) and from transmission infrared data not pre-

sented in this study, than in the case of Pt/CeO_2 pretreated similarly [1]. Particularly at $T = 523$ K, M–CO bands were poorly developed on Pd/ceria and disappeared almost completely in $CO + O_2$ (Fig. 4). At the same time, high-pressure XPS showed an oxidized PdO_2 state during the oxidizing pretreatment (Fig. 9). PdO_x is reportedly less active in CO oxidation than reduced metallic Pd [9]. Nevertheless, we found remarkable activity of preoxidized Pd/CeO_2 in CO oxidation (Fig. 1). Consequently, CO oxidation on preoxidized ceria-supported Pd and Pt does not occur in exactly the same way, because of the different affinities of Pt and Pd to oxygen. Palladium particles are oxidized and thus adsorb less CO than Pt particles. This adsorbed CO can react with oxygen from PdO_x particles, which can then be replenished by oxygen from either the gas phase or the support.

It was also concluded that in the case of Pt/CeO_2, both back spillover of oxygen from the support to the metal particles and spillover of CO (or CO_2) to the support (and/or direct adsorption of CO on the support) are possible. These processes lead to accumulation of different carbonate species on ceria, mainly bicarbonate (HCO_3^-) species on exposure to CO or $CO + O_2$ at low temperature. At higher temperatures, this species is decomposed. CO_2 is also produced in this manner (as observed by TDS as well). Accordingly, a similar reaction pathway can be suggested for Pd/ceria as well. The pronounced formation of bicarbonate species was also observed at low temperature here (Figs. 5 and 6).

Let us remember the original question of this work: "Why is Pd not active and selective in the PROX reaction (CO oxidation in the presence of H_2) even though both Pt and Pd on ceria are active in CO oxidation (without hydrogen)"? It was proposed earlier [9] that the highly active reduced Pd form (active in low-temperature CO oxidation) is oxidized to PdO_x around 360 K, which is in fact less active in CO oxidation but very active in hydrogen oxidation. It was also suggested that other metals, like Au or Pt, cannot be oxidized as easily as Pd, and that the rate of CO oxidation is higher than that of H_2 oxidation on their metallic form. This tentative proposition is not supported by any experimental evidence, however.

To clarify this issue, the differences observed in the PROX reaction between Pt/ceria (Part I [1]) and Pd/ceria (this paper) in various experiments can be summarized as follows:

(i) Pd/CeO_2 exhibited much lower selectivity toward CO_2 formation in the PROX reaction than Pt/CeO_2.
(ii) The selectivity toward CO oxidation first sharply increased as a function of temperature from 330 to 360 K, then increased slightly on Pd/CeO_2; in contrast, selectivity (from much higher values) decreased continuously as a function of temperature on Pt/CeO_2.
(iii) More hydrogen and less water desorbed from Pd than from Pt in the TDS experiment. Roughly three times more CO_2 desorbed from Pt/ceria in the first sharp TDS peak (at a temperature optimal for Pt/CeO_2 in PROX reaction).
(iv) Less CO was adsorbed on Pd than on Pt, as indicated by infrared results.
(v) At $T = 383$ K, much more formate species were found on Pd than on Pt, and their amount decreased slightly on Pd, although it increased greatly on Pt with increasing temperature. Moreover, there is a negative correlation between the intensity of the C–H stretching band of formates and the amount of CO_2 produced (see Part I [1]). In addition, formyl species were found on Pd as opposed to Pt at low temperatures, but not at higher temperatures.
(vi) More adsorbed water was found on the ceria surface of Pt/CeO_2 than on Pd/CeO_2, observed by both high-pressure XPS in the O 1s spectra (Fig. 10) and in the DRIFT spectra.
(vii) Ceria was slightly more oxidized (less reduced) at low temperatures under PROX conditions in the case of Pd/ceria than in Pt/ceria (XPS). However, this slight difference disappeared at higher temperature.
(viii) Formation of Pd β-hydride could be detected on Pd/ceria, as opposed to no hydride formation on Pt.

Based on the aforementioned differences, different reaction pathways can be proposed for ceria-supported Pd and Pt catalysts in the PROX reaction. Their simplified visualization is presented in Fig. 13. On the platinum sample at low temperature, a low-temperature water–gas shift (LTWGS)-type reaction was suggested at the Pt–ceria interface between the linearly adsorbed CO molecules (on Pt) and the adsorbed water (on ceria). As reported recently [49], such a reaction may occur directly ($COads + H_2Oads$ or OH groups) or via carboxylate intermediates, which are present in our case [1]. The byproduct hydrogen before desorption (or another hydrogen molecule from the gas phase) regenerates the water structure on the support in the close vicinity of Pt. This adsorbed water, which ensures that CO is linearly bonded to the interface Pt site, may be stabilized by the oxygen-deficient character of ceria ($CeO_{1.695}$). At higher temperatures, the hydrogen-bonded structure decomposes and water desorbs, allowing the liberation of coordinatively unsaturated (cus) Ce^{n+} sites at the interface. Thus CO can adsorb at the interface in a bridge-like manner, with oxygen coordinating to this cus site. The adsorbed CO can then dissociate or hop to the ceria and react with an OH group, forming formates. The latter species are stable on the ceria at this condition and might block the way of still existing surface water to the Pt particles. The negative correlation of surface formates and CO_2 yield strengthens the proposed model.

At low temperature ($T = 358$–385 K) in the PROX mixture, H dissolves in Pd particles, forming a hydride-like structure (Fig. 9). At the same time, CO adsorption is not hindered (Fig. 4), but CO oxidation may occur at a low rate, because the selectivity is very low. The reason for this might be that such a structure dramatically decreases the possibility of the reaction between CO adsorbed on metal particles and oxygen from either the gas phase or the support, because oxygen reacts very rapidly with H on the hydride surface during the formation of water. This water most probably desorbs or may move to the support, stabilized in a hydrogen-bonded structure similar to Pt/CeO_2 [1]. Indeed, such a structure was observed on Pd/ceria by DRIFTS (Fig. 6), but in much lower amounts than

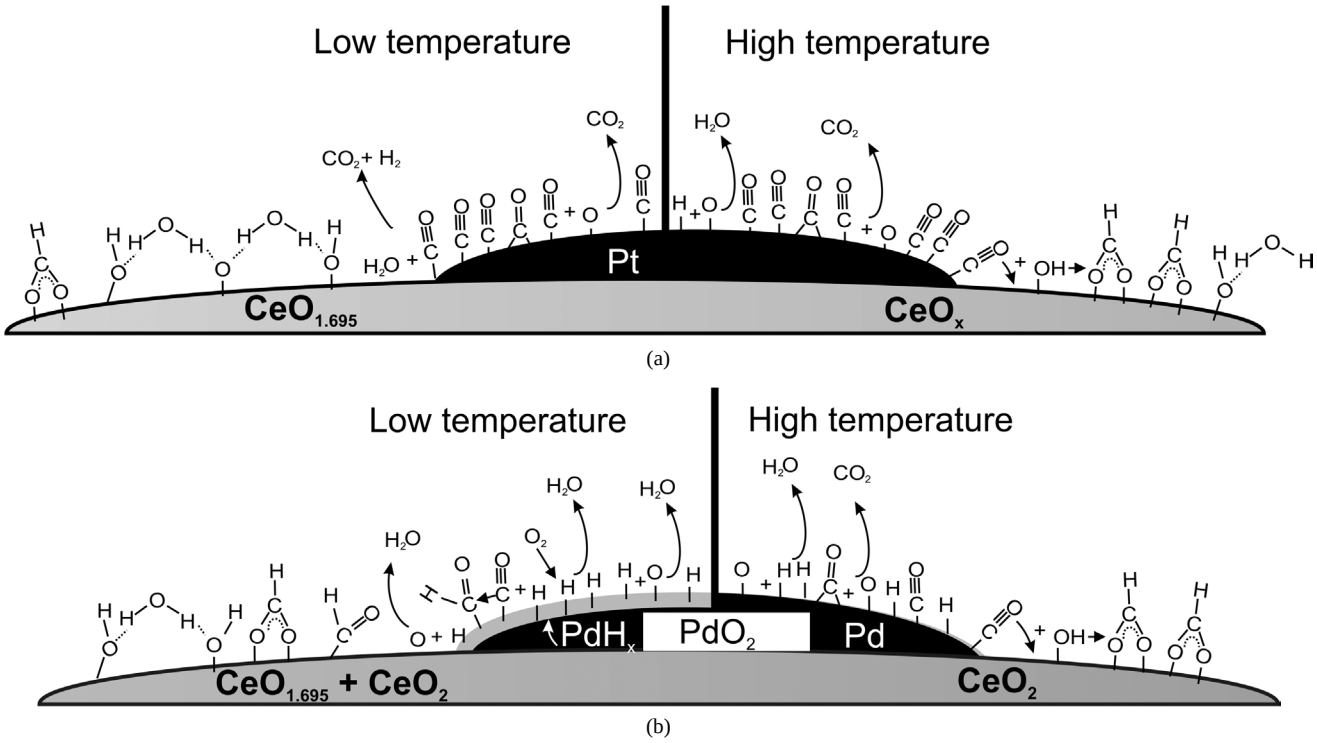

Fig. 13. Proposed models describing the reactions happening on (a), Pt/ceria and (b), Pd/ceria in the PROX reaction mixture at low and high temperature.

on Pt/ceria, as also confirmed by XPS (Fig. 11). Consequently, water preferentially desorbs from Pd under reaction conditions. The much higher affinity of palladium to hydrogen may be one reason why the hydrogen spillover to the support is less pronounced; therefore, the surface of ceria is slightly less reduced, fewer $CeO_{1.695}$ particles are found, and less water is formed and stabilized on the ceria surface as compared with the Pt/CeO_2 case. Less water on the ceria surface, less linearly adsorbed CO on Pd, and more formates probably on the way between water and CO may also contribute to the much lower activity of Pd/ceria in CO oxidation in the presence of hydrogen.

Increasing the temperature leads to decomposition of the Pd β-hydride to metallic Pd as shown by XPS (Fig. 10). Parallel to the decomposition of hydride-like structure, the selectivity toward CO oxidation increased sharply as a function of temperature up to ∼380 K, and thereafter remained almost constant with a slight increase (Fig. 2). The presence of small adsorbate-induced Pd in XPS (Fig. 9) and poorly discernable M–CO bands in DRIFTS (Fig. 4) indicate low CO coverage on the metallic Pd phase at $T = 523$ K. Consequently, metallic Pd may still adsorb hydrogen rather than CO. Furthermore, the remaining PdO_2 surface is supposed to oxidize hydrogen faster than CO [9]. These two facts might be why the selectivity toward CO oxidation is still lower on Pd/CeO_2 than on Pt/CeO_2 at high temperatures, even though no Pd-hydride phase was present here.

5. Conclusions and summary

The aims of this paper were to examine the PROX reaction on ceria-supported Pd catalyst by different (mainly in situ) experimental techniques, and also to answer the question of why both Pt and Pd catalysts are active in CO oxidation but Pd is not active in the presence of hydrogen. It is concluded that CO oxidation (without hydrogen) does not occur via the same mechanism on Pt and Pd/CeO_2 catalysts. On preoxidized Pd/CeO_2, CO is adsorbed at low coverage and reacts with oxygen from the PdO_x phase. This oxygen can then be substituted from either the gas phase or the support. On the other hand, CO coverage on Pt/CeO_2 is high, and adsorbed CO reacts with oxygen from the support. In both samples, CO spillover to the support and/or its direct adsorption and accumulation as carbonate species and ultimate desorption in the form of CO_2 is a possible reaction route in the absence of hydrogen.

In the presence of hydrogen (PROX) at low temperatures $T = 350$–380 K, formation of Pd β-hydride was evidenced from high-pressure in situ XPS. Its formation greatly suppressed the possibility of CO oxidation, because oxygen from both gas-phase and support sites (and also from PdO_x) reacts rapidly with H to form water, which desorbs easily. Nevertheless, CO adsorption was not hampered here. These entities turned partially to surface formate and formyl (–CHO) species instead of oxidation. The involvement of an LTWGS-type reaction was also hindered by less water on the ceria surface, less linearly adsorbed CO on Pd, and significantly more formate species blocking the reaction compared with Pt/CeO_2.

Increasing temperature led to decomposition of the hydride phase and a parallel increase in the selectivity toward CO oxidation. However, this remained lower on Pd/CeO_2 than on Pt/CeO_2, most probably because metallic Pd still preferentially adsorbed H to CO (low CO_{ads} signal in both DRIFTS and XPS) and the PdO_2 surface (found by XPS) preferentially oxidizes H rather than CO.

Acknowledgments

Financial support was provided by the Hungarian National Science Foundation (grant OTKA F046216), National R&D Program (NKFP 3A058-04), the Athena Consortium, and the Hungarian Academy of Sciences (a Bolyai grant to A.W.). The authors thank the BESSY staff for providing technical assistance during the in situ XPS measurements.

References

[1] O. Pozdnyakova, D. Teschner, A. Wootsch, J. Kröhnert, B. Steinhauer, H. Sauer, L. Toth, F.C. Jentoft, A. Knop-Gericke, Z. Paál, R. Schlögl, J. Catal. 237 (2006) 1.
[2] A.J. Appleby, F.R. Foulkes, Fuel Cell Handbook, Van Nostrand Reinhold, New York, 1989.
[3] C.D. Dudfield, R. Chen, P.L. Adock, Int. J. Hydrogen Energy 26 (2001) 763.
[4] S.H. Lee, J. Han, K.-Y. Lee, J. Power Sources 109 (2002) 394.
[5] G. Avgouropoulos, T. Ioannides, Ch. Papadopoulou, J. Batita, S. Hocevar, H.K. Martalis, Catal. Today 75 (2002) 157.
[6] G.K. Bethke, H.H. Kung, Appl. Catal. 194–195 (2000) 43.
[7] M.J. Kahlich, H. Gasteiger, R.J. Behm, J. Catal. 182 (1999) 430.
[8] M.M. Schubert, M.J. Kahlich, H.A. Gasteiger, R.J. Behm, J. Power Sources 84 (1999) 175.
[9] S.H. Oh, R.M. Sinkevitch, J. Catal. 142 (1993) 254.
[10] M.J. Kahlich, H.A. Gasteiger, R.J. Behm, J. Catal. 171 (1997) 93.
[11] S. Özkara, A.E. Aksoylu, Appl. Catal. A 251 (2003) 75.
[12] A. Wootsch, C. Descorme, D. Duprez, J. Catal. 225 (2004) 259.
[13] Y.-F. Han, M.J. Kahlich, M. Kinne, R.J. Behm, Phys. Chem. Chem. Phys. 4 (2002) 389.
[14] M.M. Schubert, M.J. Kahlich, G. Feldmeyer, M. Hüttner, S. Hackensberg, H.A. Gasteiger, R.J. Behm, Phys. Chem. Chem. Phys. 3 (2001) 1123.
[15] F. Marino, C. Descorme, D. Duprez, Appl. Catal. B Environ. 58 (2005) 175.
[16] W.-J. Shen, Y. Ichihashi, H. Ando, Y. Matsumura, M. Okumura, M. Haruta, Appl. Catal. A 217 (2001) 231.
[17] A. Martínez-Arias, A.B. Hungaría, M. Fernández-García, A. Iglesias-Juez, J.A. Anderson, J.C. Consea, J. Catal. 221 (2004) 85.
[18] J.A. Wang, L.F. Chen, M.A. Valenzuela, A. Montoya, J. Salamones, P.D. Angel, Appl. Surf. Sci. 230 (2004) 34.
[19] E. Bekyarova, P. Fornasiero, J. Kaspar, M. Graziani, Catal. Today 45 (1998) 179.
[20] L. Guczi, A. Beck, A. Horváth, Zs. Koppány, G. Stefler, K. Frey, I. Sajó, O. Geszti, D. Bazin, J. Lynch, J. Mol. Catal. A 204–205 (2003) 545.
[21] F. Marino, C. Descorme, D. Duprez, Appl. Catal. B 54 (2004) 59.
[22] W. Li, F.J. Garcia, E.E. Wolf, Catal. Today 81 (2003) 437.
[23] I. Rosso, C. Galletti, G. Saracco, E. Garrone, V. Specchia, Appl. Catal. B 48 (2004) 195.
[24] S. Bedrane, C. Descorme, D. Duprez, Catal. Today 73 (2002) 233.
[25] S. Bedrane, C. Descorme, D. Duprez, Catal. Today 75 (2002) 401.
[26] Y. Madier, C. Descorme, A.M. Le Govic, D. Duprez, J. Phys. Chem. B 103 (1999) 10999.
[27] D. Teschner, A. Wootsch, K. Matusek, T. Röder, Z. Paál, Solid State Ionics 141 (2001) 709.
[28] S. Kacimi, J. Barbier Jr., R. Taha, D. Duprez, Catal. Lett. 22 (1993) 343.
[29] A. Holmgren, B. Andersson, J. Catal. 178 (1998) 14.
[30] A. Palazov, C.C. Chang, R.J. Kokes, J. Catal. 36 (1975) 338.
[31] R.P. Eischens, S.A. Francis, W.A. Pliskin, J. Phys. Chem. 60 (1956) 194.
[32] F. Bozon-Verduraz, A. Bensalem, J. Chem. Soc., Faraday Trans. 1 90 (1994) 653.
[33] A. Palazov, G. Kadinov, C. Bonev, D. Shopov, J. Catal. 74 (1982) 44.
[34] A.M. Bradshaw, F.M. Hoffmann, Surf. Sci. 72 (1978) 513.
[35] A. Badri, C. Binet, J.C. Lavalley, J. Chem. Soc., Faraday Trans. 92 (1996) 4669.
[36] C. Binet, A. Badri, J.C. Lavalley, J. Phys. Chem. 98 (1994) 6392.
[37] G. Jacobs, U.M. Graham, E. Chenu, P.M. Patterson, A. Dozier, B.H. Davis, J. Catal. 229 (2005) 499.
[38] C. Li, Y. Sakata, T. Arai, K. Domen, K. Maruya, T. Onishi, J. Chem. Soc., Faraday Trans. 85 (1989) 1451.
[39] G. Busca, J. Lamotte, J.C. Lavalley, V. Lorinzelli, J. Am. Chem. Soc. 109 (1987) 5197.
[40] D. Teschner, A. Pestryakov, E. Kleimenov, M. Hävecker, H. Bluhm, H. Sauer, A. Knop-Gericke, R. Schlögl, J. Catal. 230 (2005) 186.
[41] A. Doyle, Sh. Shaikhutdinov, S.D. Jackson, H.-J. Freund, Ang. Chem. 42 (2003) 5240.
[42] G. Rupprechter, M. Morkel, H.-J. Freund, R. Hirschl, Surf. Sci. 554 (2004) 43.
[43] M.G. Ramsey, F.P. Leisenberger, F.P. Netzer, A.J. Roberts, R. Raval, Surf. Sci. 385 (1997) 207.
[44] G. Comelli, M. Sastry, L. Olivi, G. Paolucci, K.C. Prince, Phys. Rev. B 43 (1991) 14385.
[45] N. Tsud, V. Dudr, S. Fabík, C. Brun, V. Cháb, V. Matolín, K.C. Prince, Surf. Sci. 560 (2004) 259.
[46] D.R. Mullins, S.H. Overbury, D.R. Huntley, Surf. Sci. 409 (1998) 307.
[47] A.Q. Wang, P. Punchaipetch, R.M. Wallace, T.D. Golden, J. Vac. Sci. Technol. B 21 (2003) 1169.
[48] E.A. Kümmerle, G. Heger, J. Solid State Chem. 147 (1999) 485.
[49] A.B. Mhadeswar, D.G. Vlachos, J. Phys. Chem. B 108 (2004) 15246.